25th ABCM International Congress of Mechanical Engineering
October 20-25, 2019, Uberlândia, MG, Brazil

COB-2019-1149
TWO-PHASE FLOW IN A CENTRIFUGAL PUMP: HYDRAULIC HEAD AND FLOW PATTERN

Arthur Melo de Almeida
Luiz Eduardo Marinho Carneiro
Cristian Mauricio Potosi Rosero
Lívia Alves de Oliveira
Geniffer Stefany de Oliveira Martins
Atila Pantaleão Silva Freire

Universidade Federal do Rio de Janeiro

Rua Moniz Aragão N^o 360, Bloco 2, Ilha do Fundão – Cidade Universitária – Rio de Janeiro – Brasil

arthurma@poli.ufrj.br, lemcarneiro@nidf.ufrj.br, cristian.potosi@nidf.ufrj.br, liviaoliveira@nidf.ufrj.br, gmartins@nidf.ufrj.br, atila@mecanica.ufrj.br

Abstract. *The present work studies air-water flows in a commercially available centrifugal pump. The emphasis of this study is to determinate the piezometric head and identify flow patterns downstream and upstream of a centrifugal pump. The experimental hydraulic open loop is fitted with instrumentation to furnish global data on absolute pressure and flow rates. A Shadow Sizer system is also available to furnish local data, including bubble dimension, velocity and frequency.*

Keywords: *multiphase flow, centrifugal pump, flow patterns, shadow sizing*

1. INTRODUCTION

The understanding of multiphase flows behavior is essential for the development of projects in the oil, chemical and nuclear industry. The complex features of fluids that must be transported – including the presence of multiple phases – naturally impose difficult challenges on how to model the flow conditions inside the pump. The presence of multiple phases in the flow emphasizes the importance of flow patterns specification and the assessment of their effects on piezometric head deterioration, occurrence of local losses, wear of material and impact on the general operating conditions.

In the oil industry specifically, electric submersible pumps (ESP) and other pumping systems are widely used at onshore and offshore wells to artificially lift the oil and gas production. Gupta *et al.* (2015) mention that about 15% to 20% of the presently active wells produce crude petroleum with ESPs support. In particular, previous studies have shown that the gas phase inside ESPs results in degradation of the hydraulic elevation provided by the pump, pressure surges and formation of large gas bubbles, which, eventually may compromise the entire system, leading to production and financial losses. In addition to cavitation, gas accumulation may create a gas barrier that leads to total loss of pumping capability (gas lock) and overheating of the motor.

Optical techniques are a typical approach to study multiphase flows, with the benefit of not being an invasive method. This feature allows the analysis of the system without any external interference. Perissinotto *et al.* (2017), Ofuchi *et al.* (2017), Cubas *et al.* (2017) used visual techniques to study the behavior of centrifugal pumps, focusing on the two-phase flow inside the impeller and capturing the global effects of the process. In the present study, measurements through Shadow Sizing technique furnish details of the dispersed phase including information on the distribution of the size and velocity of bubbles in the suction and discharge pipes.

2. EXPERIMENTAL FACILITIES

A schematic diagram of the experimental facilities is shown in Fig. 1. The two-phase flow test section consists of a water flow loop, a separator tank, a compressed air injection system, an air-water mixer, the pipe test section (19 mm inner diameter), a progressive cavity pump (which acts as a booster) and the commercial centrifugal pump to be tested. Pressure sensors and flow meters also equip the experimental rig. The flow loop was designed primordially to acquire

global data (including the absolute pressure and temperature inside of the testing tube near the pump) so as to compare the single and two phase performance curves. To understand the phase distribution to which the flow in the pump is being submitted, the pipes are transparent.

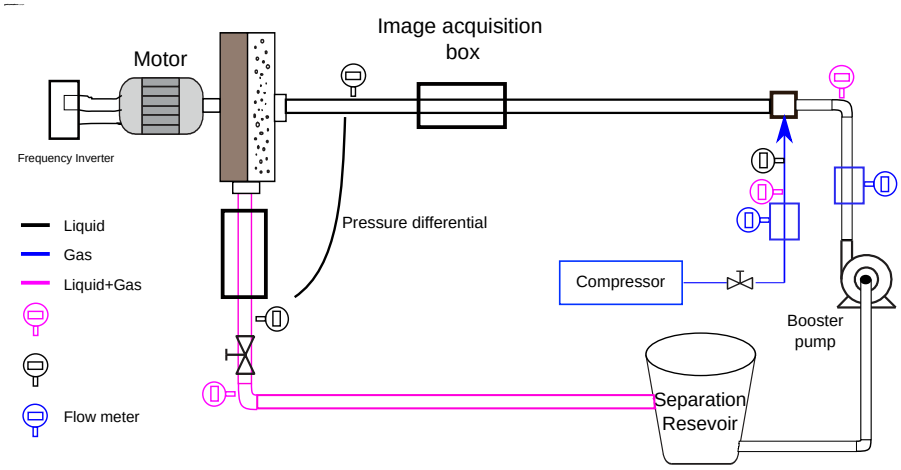

Figure 1: Schematic drawing of the experimental setup. Adapted from Cubas *et al.* (2017).

The gas flow ratio, β , is calculated through the measured and adjusted volume flow of each phase. Consider Q_L the liquid flow and Q_G the gas flow in m^3/h. Defined as:

$$\beta = \frac{Q_G}{Q_L + Q_G} \tag{1}$$

As a result of changes in specific volume of the gas phase, the gas-liquid ratio can change downstream of the flow due to pressure drop or increment. In this case, Q_G needs to be adjusted for each observed location since changes in β arise. For Q_L, it is considered that the liquid phase is incompressible so that changes are negligible.

The Shadow Sizing system consists of a computer, a timer box (used to synchronize the equipment), a high speed camera (located in front of the test section) and a LED light set (in the background opposite to the camera), as shown in Fig. 2a. This technique allows the identification of the contour of the bubbles due to the shadow created by the light source, and after post-processing the recorded images, it is possible to calculate bubble size distribution, velocity and other statistically relevant properties of the dispersed phase.

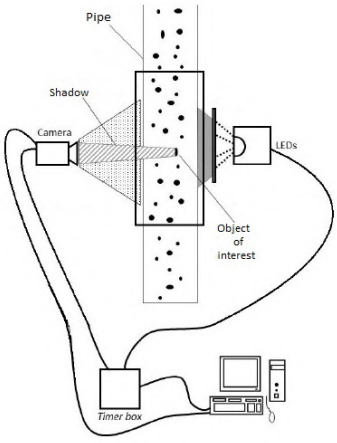

(a) Shadow sizing system. Gavioli (2017)

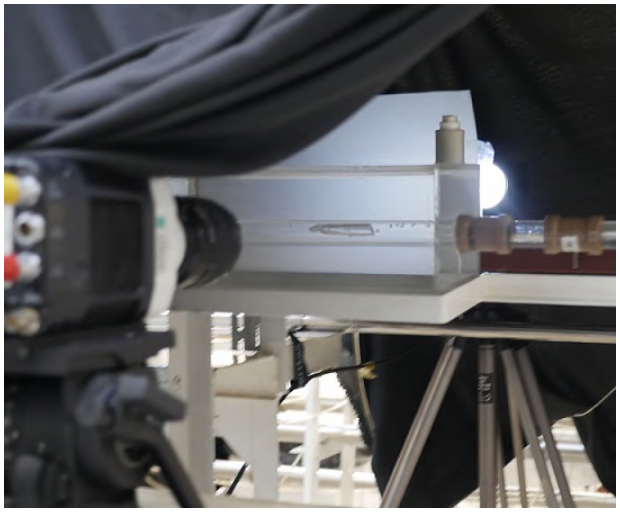

(b) Shadow sizing equipment

Figure 2: Image acquisition and shadow sizing equipment

Due to the curvature of the tube, light refraction distorts the observed image as light travels through three different mediums. To mitigate this effect, an observation box was designed to compensate most of the distortion. This observation

box contains the analyzed tube inside it and it is filled with denatured water directing the incoming light to a mostly perpendicular configuration to the camera (Fig. 2b).

Experiments were conducted in three phases: 1- Centrifugal pump performance curves for monophasic water flow were measured and plotted; 2- Pump performance curves for biphasic air-water flow were measured and Phase 3- Shadow Sizing imaging to identify the flow pattern for different conditions of biphasic flow and its changes caused by the pump. Phase 1 was conducted to acquire comparison points for Phase 2 data. In the second phase, four predefined impeller rotation speeds were selected and for each rotation, comparative head curves were measured for specific β values ranging from a minimum of 0.005 up to 0.12 depending on the experimental conditions.

In the experimental procedure, each assessment point was set with values of incoming Q_G adjusted by downstream pressure values so that the gas flow ratio on the inlet of the pump was kept in the desired value.

3. EXPERIMENTAL RESULTS

To assess the pump performance under single phase flow, the piezometric head curves were obtained for four different rotational speeds. The frequency interval chosen for the experiments was 20 Hz (1173 rpm) to 40 Hz (2347 rpm), to avoid low rotational speeds and the associated high measurement uncertainties and assure sufficiently high pressure drops. Two other rotation speeds were selected in between the two extremes of the operating range so as to allow a better representation of the phenomenon: 1643 rpm (28Hz) and 2053 rpm (35Hz).

The measured pump single phase piezometric head for each frequency can be seen in Fig. 3a. Pressure increment points due to single phase water flow were obtained for different rotation speeds. The points were fitted through curves with acceptable coefficients of determination ($R^2 > 0.9973$).

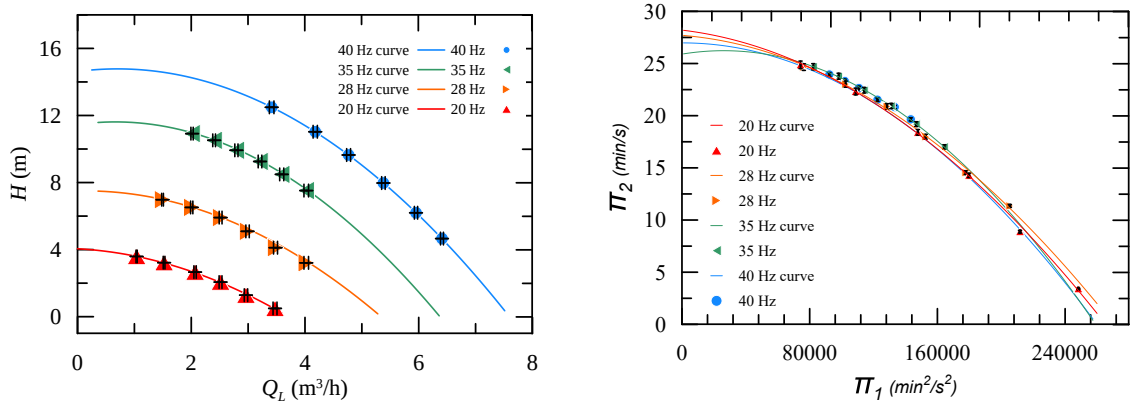

(a) Experimental single phase piezometric head for different speeds.

(b) Comparison for different frequencies at the centrifugal pump.

Figure 3: Single phase experimental analysis

All the single phase experimental curves collapse with the use of the dimensionless numbers: head and flow coefficient, Equations 2 and 3 respectively. As seen in Fig. 3b, the expected similarity is observed for all frequencies.

$$\pi_1 = \frac{Q}{ND^3} \tag{2}$$

$$\pi_2 = \frac{gH}{N^2D^2}. \tag{3}$$

Even though π_1 and π_2 have dimensionless significance, they have units related to industry usage. SI units were used for the gravity acceleration, volume flow, diameter, and the piezometric head, while for the pump rotation (N) rotations per minute were used per industry standard.

The second phase of the experimental campaign consisted in the acquisition of additional data for different gas-liquid flow ratio to study the effects of air fraction in the piezometric head curves for every rotation speed as shown in Fig. 4.

The curves shown in Fig. 4 are similar in format to those observed by Gamboa (2008); Monte Verde *et al.* (2017); Ofuchi *et al.* (2017), albeit different rotational speeds and pressure increments. Surging and gas blockage behavior of the centrifugal pumps were observed for values of $\beta > 0,005$. In the experiments for global data, the presence of a critical liquid flow value Q_{Lcrit} for each β and rotational speed was noticed. Below this critical liquid flow rate, the pump struggles to produce head. For higher values, a sudden recovery of the pressure increase capacity is noted. Around the point of critical liquid flow, the measured head fluctuated between two plateaus, suggesting the presence of a flow transition between two patterns: (i) gas pocket or (ii) separated flow inside the pump impeller Monte Verde *et al.* (2017).

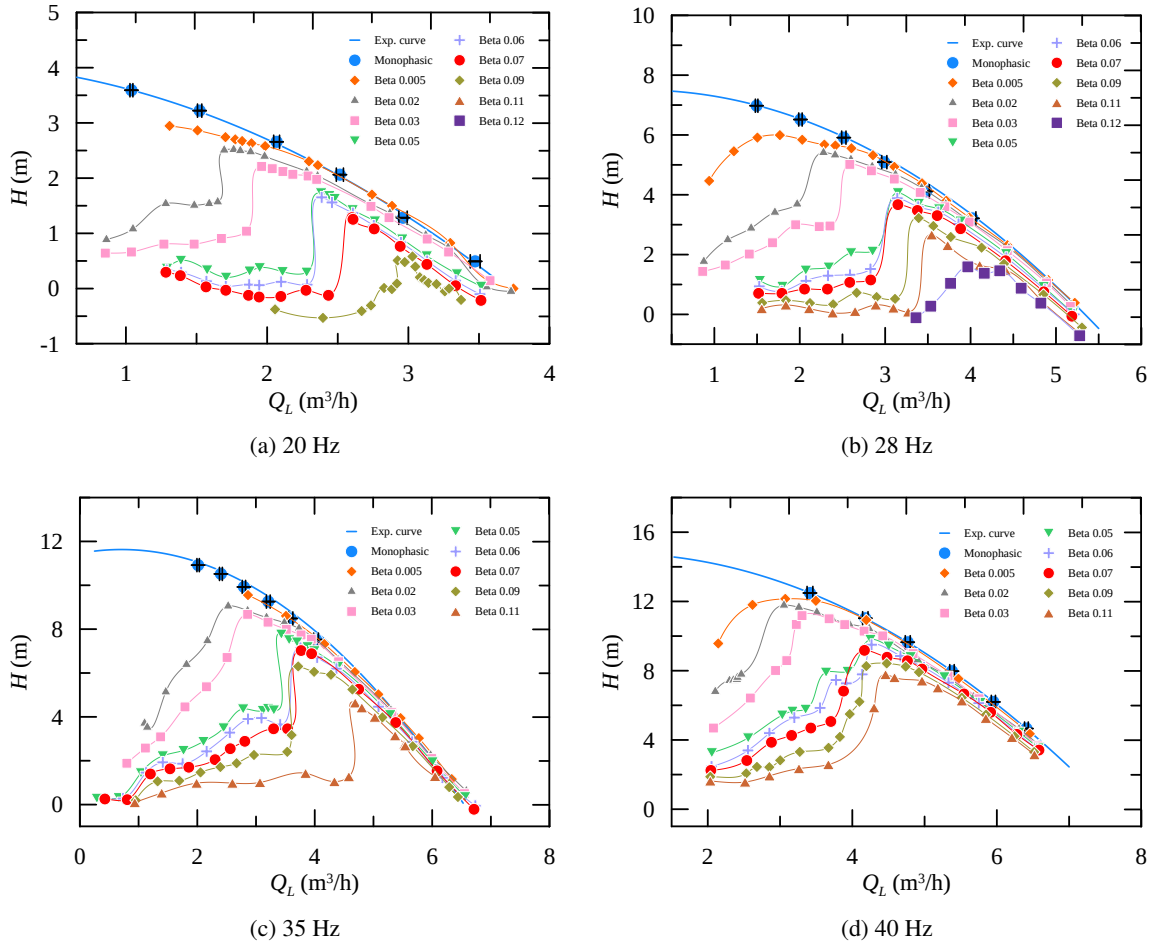

(a) 20 Hz (b) 28 Hz

(c) 35 Hz (d) 40 Hz

Figure 4: Experimental piezometric head curve for different gas ratios and rotational speeds. Data on single phase water flow is also shown for comparison.

In Phase 3, several images of the two phase flows were obtained with a high speed camera and LED at both inlet and outlet conditions. Both equipment were synchronized trough a timer box and activated via a specialized computer software as shown in Fig. 2b. The experiments aimed at studying the type of two-phase flow ratios encountered by the pump in two different rotation speeds to evaluate the flow pattern changes caused by the centrifugal pump, as can be observed in the almost linear sequence of points in Fig. 5. Most of the observed points with similar gas-liquid ratio fall into the pattern of elongated bubble flow or dispersed bubble flow. To expand the results, the shadow sizing technique was also performed for flow conditions outside of the pump's recommended operational conditions. The purpose was to observe any existing drastic pattern change. These experiments were carried out with much higher gas-liquid ratio so that the presence of intermittent patterns such as slug flow are observed.

The flow patterns immediately upstream and downstream of the centrifugal pump can be observed and compared to the pattern map in Fig. 5. They show no significant change in its position on the map after having its gas flow rate corrected by the pressure change. An evident observation of the Shadow Sizing images is that the centrifugal field violently breaks up bubbles, reducing the slug flow pattern to a transient meta-stable dispersed bubble mixed with slug pattern amidst a correlated reduction of slug length downstream of the pump in comparison to its upstream properties.

Images of the multiphase flow pattern obtained through the Shadow Sizing system are shown in Fig. 6. This case represents an air-water flow with same conditions of flow rates and $\beta = 0,05$.

Bubble pattern is observed in both pump frequencies upstream of centrifugal pump. Downstream of the pump, dispersed bubbles are observed. These bubbles are smaller than those observed in the inlet of the pump. Fig. 7 shows the bubble diameter and velocity distributions in both locations to illustrate the flow behavior change due the centrifugal pump.

In Fig. 7a both diameter distributions for the frequencies display a good agreement as compared with the pattern identified by the Shadow Sizing system. The bubble diameter distribution function at the pump outlet decreases relative to the pump inlet. Consequently, it is possible to infer that a smaller size presented in the pattern comes from the bubble breakup producing a larger number of bubbles. In this case, the pump frequency does not influence the diameter distribution, for

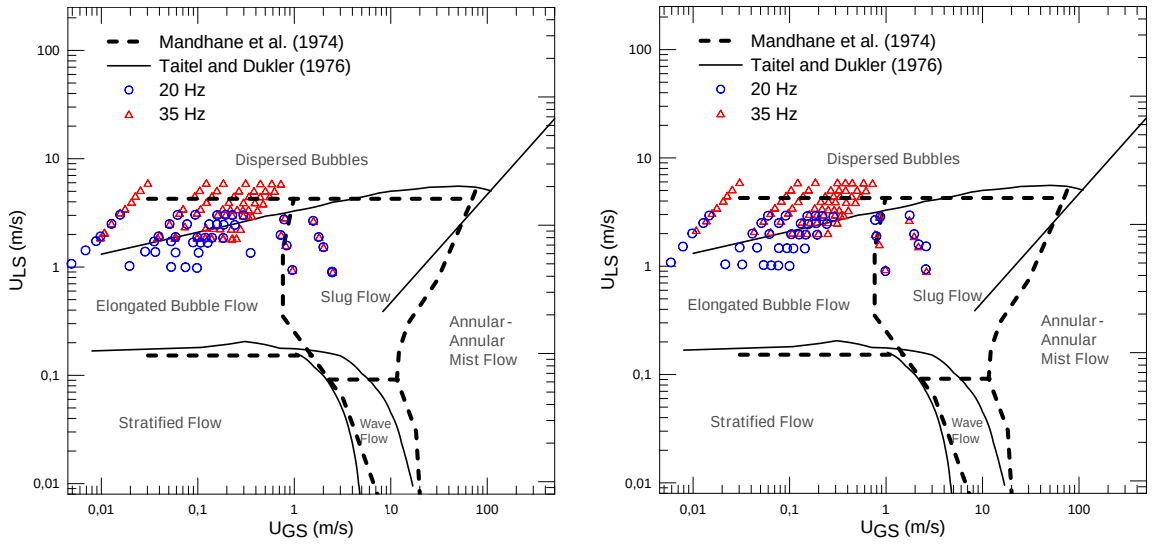

(a) Upstream conditions

(b) Downstream conditions

Figure 5: Selected experimental points acquired via Shadow Sizing in their conditions before and after the pump plotted over the flow pattern maps of Taitel and Dukler (1976) and Mandhande *et al.* (1974).

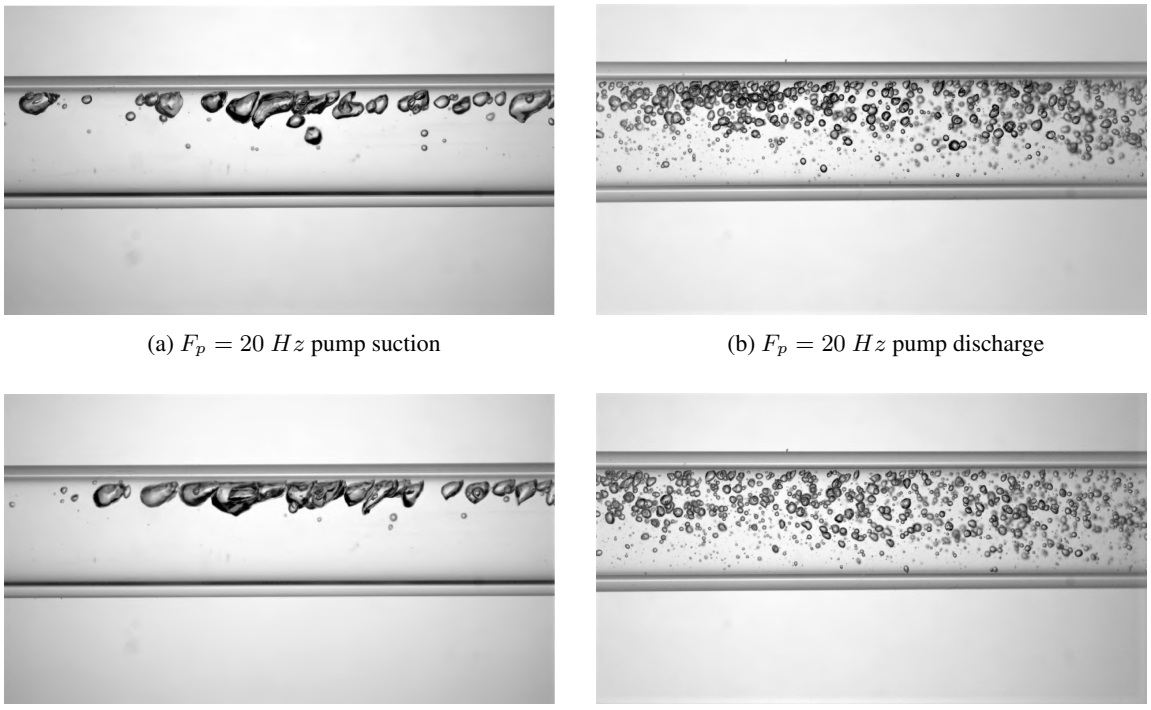

(a) $F_p = 20\ Hz$ pump suction

(b) $F_p = 20\ Hz$ pump discharge

(c) $F_p = 35\ Hz$ pump suction

(d) $F_p = 35\ Hz$ pump discharge

Figure 6: Shadow imaging for $Q_L = 2,0 m^3/h$ and $Q_G = 0,1 m^3/h$ for two pump frequencies.

both frequency the curves are very closed to each other.

The curves of velocity distribution Fig. 7b have shown influence by the pump frequency and by the flow position in the upstream and downstream of the centrifugal pump. The lower pressure values at the pump's inlet result in higher bubble velocities. In the outlet the pump, the velocities increase due the supplied head.

An important aspect to note is the behavior of an elongated bubble passing through the centrifugal pump. Table 1 shows the average slug length, speed and frequency of slug flow at the inlet and outlet of the centrifugal pump. Q_G values were adjusted according to pressure and temperature at each point. In some cases there is a change of β values before and after the pump due to the line pressure increment or decrement depending on whether the pump is producing head or not. In the case of the Table 1 acquisitions, there was a negligible change in gas flow.

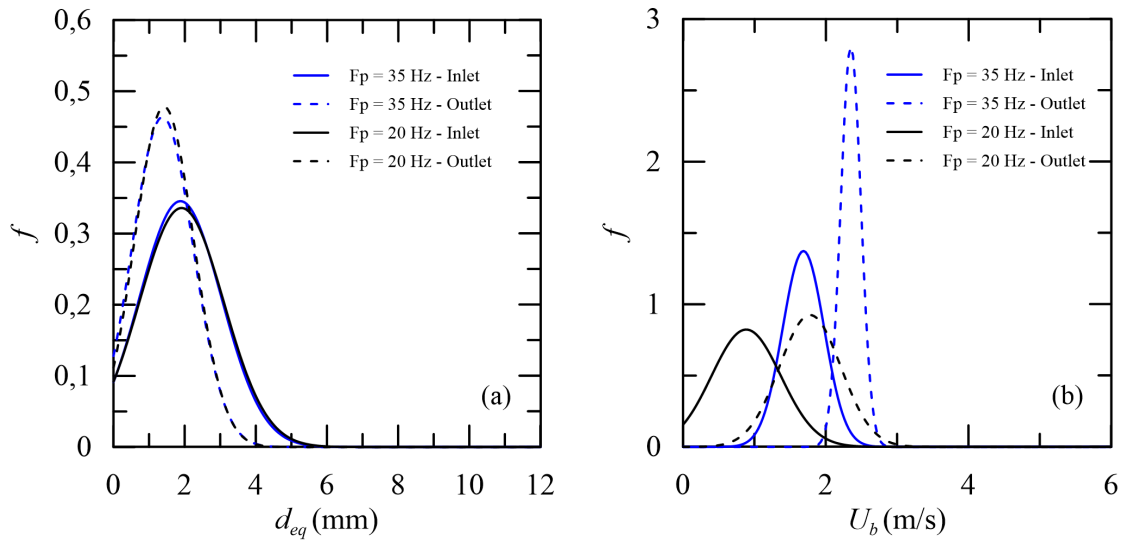

(a) Equivalent diameter

(b) Velocity

Figure 7: Distributions for bubbly pattern. $Q_L = 2,0\ m^3/h$ and $Q_G = 0,1\ m^3/h$.

Location	$F_p\ (Hz)$	$Q_L\ (m^3/h)$	$Q_g\ (m^3/h)$	$\overline{L_{slug}}\ (mm)$	$\overline{V_{slug}}\ (m/s)$	$\overline{f_{slug}}\ (s^{-1})$
Inlet	20	0,958	0,974	69,07	0,51	4,63
Outlet	20	0,958	1,005	42,47	0,61	1,76
Inlet	35	0,958	0,979	82,05	0,55	4,30
Outlet	35	0,958	1,006	21,90	0,53	3,99

Table 1: Slug properties change for two different rotational speeds at $Q_L = 0,958\ (m^3/h)$ and $\beta \approx 0,50$

It was perceived a length increment of the slug pattern flow in the region upstream of the centrifugal pump, thus its slug flow frequency was much higher compared to that observed immediately after the centrifugal pump. This can be explained by the fact that the centrifugal pump breaks large bubbles into small bubbles even decreases the number of slugs, as can be seen in Fig. 8. The statistics of these figures are shown in Table 1.

Another observation was the appearance of a flow pattern consisting of an combination of three different simultaneous flow regimes. The first was identified as dispersed bubbles, mainly present in the wake region of the slug flow. This condition has been shown in Fig. 9a. For Fig. 9b, a transition pattern in which elongated bubbles are present is observed, suggesting the flow recovers a slugs flow pattern downstream. The third pattern is identified as slug pattern (Fig. 8d), for both pump frequencies. It should be noted that the slugs at pump outlet have an unclear or distorted noses, which renders the clear determination of the slug lenght difficult.

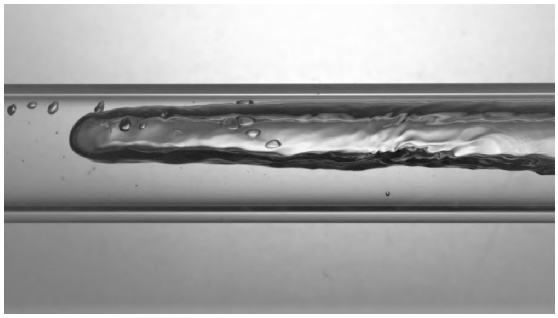

(a) $F_p = 20\ Hz$ pump suction

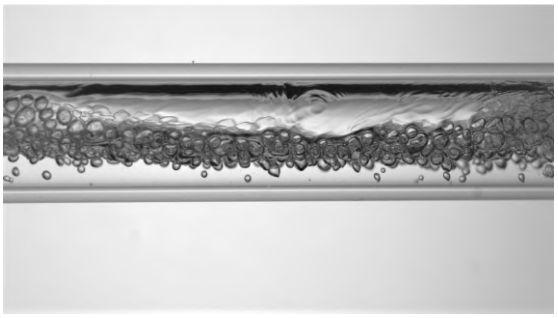

(b) $F_p = 20\ Hz$ pump discharge

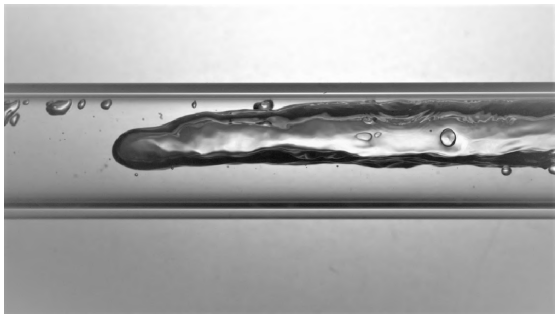

(c) $F_p = 35\ Hz$ pump suction

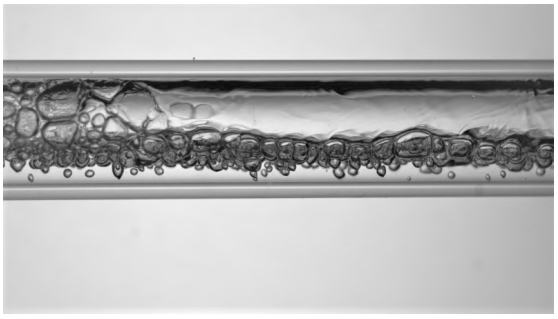

(d) $F_p = 35\ Hz$ pump discharge

Figure 8: Air-water flow, $Q_L = 0.958m^3/h$, $Q_{G-inlet} = 0.97m^3/h$ and $Q_{G-outlet} = 1.0m^3/h$ for two pump frequencies.

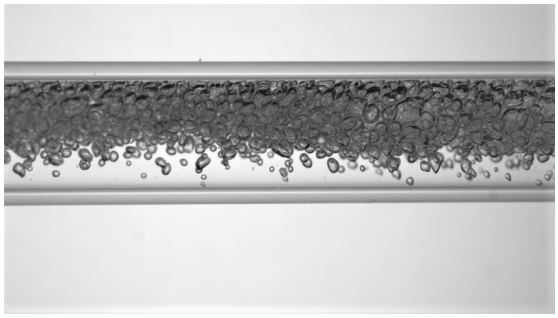

(a)

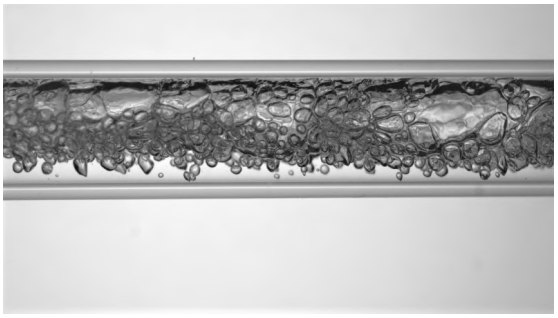

(b)

Figure 9: Transition pattern in air-water flow $Q_L = 0.958m^3/h$ and $Q_{G-outlet} = 1.0m^3/h$ for pump outlet. $F_p = 35Hz$

4. ACKNOWLEDGEMENTS

The authors are grateful to Petrobras for the financial support received during realization of the work.

5. REFERENCES

Cubas, J.M.C., Stel, H., Ofuchi, E.M., Bertoldi, D., Neto, M.A.M. and Morales, R.E.M., 2017. "Experimental analisis of two-phase in a radial centrifugal pump". *24th ABCM International Congress of Mechanical Engineering*, Vol. December 3-8, pp. Curitiba, PR, Brazil.

Gamboa, J., 2008. *PREDICTION OF THE TRANSITION IN TWO-PHASE PERFORMANCE OF AN ELECTRICAL SUBMERSIBLE PUMP*. Ph.D. thesis.

Gavioli, Y.S., 2017. *Caracterização experimental da separação gás-líquido em uma junção do tipo T inclinada*. Master's thesis, Universidade Federal do Rio de Janeiro, Rio de Janeiro, Brazil.

Gupta, S., Nikolaou, M., Saputelli, L. and Panjwani, S., 2015. "Applying predictive analytics to detect and diagnose impending problems in electric submersible pumps used for lifting oil from wellbores". *AIChE Annual Meeting Proceedings (ISBN: 978-0-8169-1094-6)*.

Mandhande, J.M., Gregory, G. and Aziz, K., 1974. "A Flow Pattern Map for Gas-Liquid Flow in Horizontal Pipes". *Int.*

J. Multiphase Flow, Vol. 1, No. 4, pp. 537–553.

Monte Verde, W., Biazussi, J.L., Sassim, N.A. and Bannwart, A.C., 2017. "Experimental study of gas-liquid two-phase flow patterns within centrifugal pumps impellers". *Experimental Thermal and Fluid Science*, Vol. 85, pp. 37–51. doi:http://dx.doi.org/10.1016/j.expthermflusci. 2017.02.019.

Ofuchi, E.M., Ancajima, F.C., Sabino, R.G.H., Stel, H., Bertoldi, D., Neto, M.A.M. and Morales, R.E.M., 2017. "Influence of operational conditions on the air bubble dynamics inside a centrifugal pump". *24th ABCM International Congress of Mechanical Engineering*, Vol. December 3-8, pp. Curitiba, PR, Brazil.

Perissinotto, R.M., Verde, W.M., de Castro, M.S. and Bannwart, A.C., 2017. "Experimental investigation of forces acting on oil drops within esp impellers". *24th ABCM International Congress of Mechanical Engineering*, Vol. December 3-8, pp. Curitiba, PR, Brazil.

Taitel, Y. and Dukler, A., 1976. "A Model for Predicting Flow Regime Transistion in Horizontal and Near Horizontal Gas-Liquid Flow". *AIChE Journal*, Vol. 22, No. 1, pp. 47–55.